# Object Recognition Using Mechanical Impact, Viscoelasticity, and Surface Friction During Interaction

Pakorn Uttayopas, Xiaoxiao Cheng, Jonathan Eden, *Member, IEEE*, and Etienne Burdet

***Abstract*—Current robotic haptic object recognition relies on statistical measures derived from movement dependent interaction signals such as force, vibration or position. Mechanical properties, which can be estimated from these signals, are intrinsic object properties that may yield a more robust object representation. Therefore, this paper proposes an object recognition framework using multiple representative mechanical properties: stiffness, viscosity and friction coefficient as well as the coefficient of restitution, which has been rarely used to recognise objects. These properties are estimated in real-time using a dual Kalman filter (without tangential force measurements) and then are used for object classification and clustering. The proposed framework was tested on a robot identifying 20 objects through haptic exploration. The results demonstrate the technique's effectiveness and efficiency, and that all four mechanical properties are required for the best recognition rate of 98.18 ± 0.424%. For object clustering, the use of these mechanical properties also results in superior performance when compared to methods based on statistical parameters.**

***Index Terms*—Haptic exploration, interaction mechanics, feature extraction, supervised learning for classification, clustering.**

## I. Introduction

As ROBOTS are increasingly used in various fields e.g. agriculture, they have to manipulate objects of different mechanical properties skillfully. For instance, to harvest tomatoes or potatoes with similar shape, it is necessary to know their respective mechanical properties to handle them without dropping or crushing them. To recognize the objects a robot is interacting with, the unique features that characterise them need to be extracted [1]. While geometric features can be used to identify solid objects [2], [3], [4], the shape of compliant objects changes with interaction such that shape alone is insufficient for identification.

Compliant objects can be recognised by using tactile information obtained during haptic interaction such as force and vibrations. Empirical measures of these signals, such as the maximum, minimum and variance have been used for classification [5], [6], [7]. While these interaction features can be employed for object recognition, their value depends on specific actions, and the information that they provide can be redundant leading to high computational costs.

The intrinsic mechanical features, which describe an object's behavior in response to a load, may yield a specific representation and lead to more efficient object recognition. For example, the coefficient of restitution can characterise the energy loss [8] during an impact. Furthermore, viscoelasticity can describe the deformation and restoration of the surface in response to a perpendicular force, while when applying a tangential force, roughness can represent the resistance to sliding. These parameters have been previously estimated as mechanical properties from tactile information.

The coefficient of restitution is an important property in characterising how a surface material reacts during an impact. While this property has rarely been used for object recognition, related features have been extracted from the frequency spectrum of acoustic and acceleration signals [9], [10] or applying unsupervised learning methods [11] or statistical tools [12], [13]. The acceleration peak has also been considered as a similar impact related feature for object recognition, proving able to recognise five different materials [14].

Compliance-related features characterise the deformation in response to continuous forces. Empirically, these features can be estimated by analyzing the normal force signal during interaction [7], [15], [16]. Such approaches have been used to estimate stiffness [17], [18] and to infer how full a bottle is in grasping [19]. Stiffness, however, only characterises the static response. To estimate both stiffness and viscosity, recursive least-square algorithms [20], [21], [22] and a Gaussian process [23] have been used. These estimated features have then been applied to object recognition in simulation [24].

To characterise the response to sliding, roughness related features are often used. These features are typically estimated

Manuscript received 20 October 2022; revised 2 March 2023; accepted 7 April 2023. Date of publication 26 April 2023; date of current version 20 June 2023. This work was supported in part by the U.K. EPSRC EP/N029003/1 MOTION Project, and in part by the EC under Grants FETOPEN 829186 PH-CODING and ITN PEOPLE 861166 INTUITIVE. This paper was recommended for publication by Associate Editor Hiroyuki Kajimoto and Editor-in-Chief Domenico Prattichizzo upon evaluation of the reviewers' comments. *(Corresponding authors: Xiaoxiao Cheng; Etienne Burdet.)*

Pakorn Uttayopas, Xiaoxiao Cheng, and Etienne Burdet are with the Department of Bioengineering, Imperial College of Science, Technology and Medicine, W12 0BZ London, U.K. (e-mail: pu18@imperial.ac.uk; xiaoxiao.cheng@imperial.ac.uk; e.burdet@imperial.ac.uk).

Jonathan Eden was with the Department of Bioengineering, Imperial College of Science, Technology and Medicine, W12 0BZ London, U.K. He is now with the Mechanical Engineering Department, the University of Melbourne, Parkville, VIC 3010, Australia (e-mail: j.eden@imperial.ac.uk).

This article has supplementary downloadable material available at https://doi.org/10.1109/TOH.2023.3267523, provided by the authors.

Digital Object Identifier 10.1109/TOH.2023.3267523

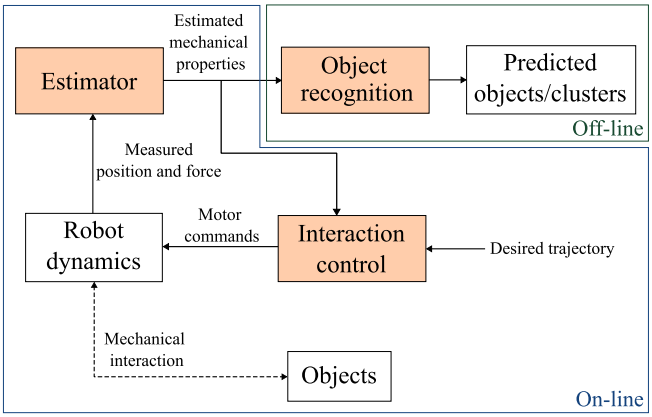


Fig. 1. Object recognition process. The end-effector force and position measured during interaction are used to obtain mechanical properties with an estimator (Sections II-A,B,C). The estimated mechanical features are then used to recognize objects (Section IV) and adjust the motor command with the controller (Section II-D).

from the force or vibration occurring in the tangential direction during sliding [25], [26], [27]. A constant Coulomb model is commonly used to identify surface friction [28], [29]. Using the surface friction along with geometrical information, 18 household objects with different shapes and materials could be recognised [30]. The robot-environment interaction can also be modelled using a quasi-static LuGe model [31] for the inclusion of dynamic friction parameters, which have been shown to benefit the classification of objects with different surface materials [32], [33].

These previous works show how a single mechanical property can benefit object recognition. However, a given mechanical property may have identical values across multiple objects (e.g., having similar stiffness for two solid materials) and thus they cannot be distinguished by it solely. Integrating a collection of mechanical property estimations may improve object recognition. However, there is currently no such haptic exploration framework to estimate the viscoelasticity, friction, and especially the coefficient of restitution systematically and use them together for object recognition.

This prompted us to develop a framework for the estimation of mechanical properties and investigate their use to recognise specific objects. In this new approach, the coefficient of restitution, stiffness, viscosity and friction coefficient are estimated from the interaction force during haptic exploration. Our work builds upon [34] which adapted viscoelastic parameters to maintain a stable interaction. To address issues with the parameter oscillation in [34] we used a dual Kalman filter to consider sensory noise. We further incorporated the estimation of the coefficients of friction and restitution. The resulting method is first validated in simulation. The role of each mechanical parameter in object recognition is then investigated before our method is compared to representative statistical and empirical methods.

Fig. 1 shows the overall recognition framework with its three components; estimation, control, and recognition. A robot, driven by a controller, interacts mechanically with objects to retrieve the corresponding interaction forces at different locations. The robot estimator first estimates the coefficient of restitution when touching the object's surface (details in Section II-B). A dual extended Kalman filter (DEKF) is then used to estimate the object stiffness, viscosity and friction coefficient online from signals of haptic sensors (Section II-C). These mechanical features are also used to adapt the controller parameters so as to interact with each object properly (Section II-D). After haptic exploration, the features consisting of the estimated mechanical parameters are combined to form a dataset feeding object recognition algorithms to identify and cluster objects offline (Section IV).

## II. Online Estimation and Control

This section describes the online estimation and control. First, a discrete impact model and a continuous interaction model are introduced to capture the robot-environment interaction at different stages. Using these models, the estimation of impact (coefficient of restitution) and continuous interaction properties (stiffness, viscosity and friction coefficient) are presented. Finally, the interaction controller used to smoothly drive the robot interaction with the environment is explained.

### A. Interaction Model

Let the dynamics of a $n$-DOF robot interacting with its environment be described by

$$M(q)\ddot{x} + C(q,\dot{q})\dot{x} + G(q) \;=\; u + F + \omega\,, \tag{1}$$

where $x$ is the coordinate of the end effector in operational space and $q$ is the joint angle vector. $M(q)$ and $C(q,\dot{q})$ represent the inertia and Coriolis matrices and $G(q)$ the gravitation vector, $u$ is the control input and $\omega$ motor noise. The interaction force $F$ can be modelled with a mass-spring-damper system in the normal direction and Coulomb friction in the tangential direction:

$$F = \begin{bmatrix} F_\perp \\ F_\parallel \end{bmatrix} = \begin{bmatrix} F_0 + \kappa\, x + d\,\dot{x} \\ \mu F_\perp \end{bmatrix}, \tag{2}$$

where $F_\perp$ and $F_\parallel$ are the interaction forces in the normal direction $\perp$ and tangential direction $\parallel$ respectively, $F_0 = -\kappa\, x_0$ is the force corresponding to the surface rest length $x_0$ (without interaction), $\kappa$ is the surface stiffness, $d$ its viscosity, and $\mu$ its friction coefficient.

### B. Impact Estimation

The initial contact of a robot with an object occurs in two phases: deformation and restoration. The deformation phase occurs before the initial point of contact and continues until maximum deformation. Then restoration occurs until separation. The coefficient of restitution is defined as the ratio of the normal impulse of restoration to the normal impulse of deformation [35]:

$$\widehat{\psi} = \frac{R}{D} = \left| \frac{\int_{t^0}^{t^+} F_\perp\, dt}{m_\perp[\dot{x}_\perp(t^-) - \dot{x}_\perp(t^0)]} \right|. \tag{3}$$

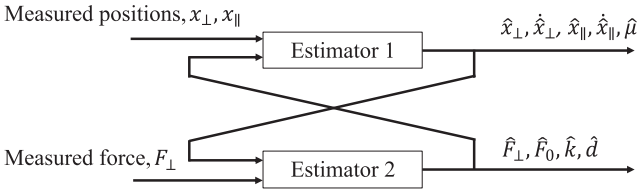


Fig. 2. Dual extended Kalman filter. At each time step, Estimator 1 obtains the robot states and friction coefficient from the measured position and estimated interaction force. Estimator 2 obtains the object viscoelasticity parameters and interaction force from the measured force and estimated robot states.

where $D$ is the momentum from 0.01 s before collision, $t^-$, to the time of maximum deformation, $t^0$, and $R$ integrates the normal force from $t^0$ to 0.01 s after collision, $t^+$.

### C. Continuous Properties Estimation

We assume that the robot can measure the end-effector position (e.g. from joint encoders) as well as the force normal to the surface subjected to a noise $\nu$.

The estimated system dynamics become nonlinear due to the coupling of the robot states and mechanical parameters in the interaction force model (2). In discrete state-space form, the dynamics of the robot interacting with the environment is:

$$\begin{aligned} \xi_{k+1} &= f(\xi_k, u_k, \theta_k) + \omega_k \\ \eta_k &= h(\xi_k) + \nu_k \\ \xi \equiv \begin{bmatrix} x_\perp \\ \dot{x}_\perp \\ x_\parallel \\ \dot{x}_\parallel \\ \mu \end{bmatrix}, \quad \eta &\equiv \begin{bmatrix} x_\perp \\ x_\parallel \end{bmatrix}, \quad u \equiv \begin{bmatrix} u_\perp \\ u_\parallel \end{bmatrix}, \quad \theta \equiv \begin{bmatrix} F_0 \\ k \\ d \end{bmatrix} \end{aligned} \tag{4}$$

where $f$ is a nonlinear mapping obtained from (1) and $h$ is a nonlinear mapping between the states and observation. The augmented state $\xi$ consists of the robot states and the friction parameter, $u$ are motor commands, $\eta$ is the measured robot positions and $\theta$ is the viscoelasticity vector.

Due to the system's nonlinearity, noise and the coupling between the states and parameters, we employ the dual extended Kalman filter method of [36] to estimate the robot states and interaction mechanics' parameters simultaneously. The dual Kalman filter is a recursive estimation process, which uses partial measurements to estimate the parameters in the model before integrating the updated model and measurements to estimate the unobservable states. Fig. 2 depicts the two designed estimators. Estimator 1 estimates the state $\xi$, which includes the robot states and the friction parameter. Estimator 2 then estimates the viscoelasticity parameters $\theta$ from the measured normal force. In principle, the prediction error is minimized when the estimated parameters $\hat{\theta}, \hat{\mu}$ converge on the real values $\theta, \mu$ while the estimated states $\hat{\xi}$ converge to the real states $\xi$.

*1) Robot States Estimation:* The robot states $\xi$ and friction parameter $\mu$ are estimated together by using the nonlinear stochastic state-space model (4), with the linearization

$$\begin{aligned} \xi_{k+1} &= A_k\, \xi_k + B_k\, u_k + \omega_k \\ \eta_k &= C_k\, \xi_k + \nu_k \end{aligned} \tag{5}$$

$$A_k = \left.\frac{\partial f(\xi, u, \theta)}{\partial \xi}\right|_{(\hat{\xi}_k, \hat{\theta}_k, u_k)} = \begin{bmatrix} 1 & \triangle & 0 & 0 & 0 \\ 0 & 1 & 0 & 0 & 0 \\ 0 & 0 & 1 & \triangle & 0 \\ 0 & 0 & 0 & 1 & \hat{F}_{\perp k}\triangle/m_\parallel \\ 0 & 0 & 0 & 0 & 1 \end{bmatrix},$$

$$B_k = \left.\frac{\partial f(\xi, u, \theta)}{\partial u}\right|_{(\hat{\xi}_k, \hat{\theta}_k, u_k)} = \begin{bmatrix} 0 & 0 \\ \triangle/m_\perp & 0 \\ 0 & 0 \\ 0 & \triangle/m_\parallel \\ 0 & 0 \end{bmatrix},$$

$$C_k = \left.\frac{\partial h(\xi)}{\partial \xi}\right|_{(\hat{\xi}_k, \hat{\theta}_k, u_k)} = \begin{bmatrix} 1 & 0 & 0 & 0 & 0 \\ 0 & 0 & 1 & 0 & 0 \end{bmatrix},$$

where $m_\perp$ and $m_\parallel$ are the mass matrix components in the normal and tangential directions, respectively, and $\triangle$ is the integration time step. $\hat{F}_\perp$ is the estimated normal force from the environment model (2). The Kalman Filter to estimate $\xi$ is then designed as

$$\hat{\xi}_{k+1} = \hat{\xi}^-_{k+1} + K_{\xi,k+1}\left(\eta_k - C\hat{\xi}^-_{k+1}\right) \tag{6}$$

where $\hat{\xi}^-_{k+1} = f(\hat{\xi}_k, u_k, \hat{\theta}_k)$ is the predicted states obtained by using the last estimated states and $K_{\xi,k+1}$ is the filter gain for state estimation.

*2) Viscoelasticity Parameters Estimation:* The viscoelasticity parameter $\theta$ can be estimated using the measured normal force, the interaction force model (2) and the estimated robot states $\hat{\xi}$. An EKF is used to estimate viscoelasticity parameters by considering the following state-space model:

$$\begin{aligned} \theta_{k+1} &= \theta_k + \omega_k \\ \eta_{\theta,k} &= h_\theta\left(\xi_k, \theta_k\right) + \nu_k\,. \end{aligned} \tag{7}$$

The observer for the estimation of viscoelasticity parameters is given by:

$$\hat{\theta}_{k+1} = \hat{\theta}_k + K_{\theta,k+1}(\eta_{\theta,k} - C_{\theta,k}\hat{\theta}_k) \tag{8}$$

where $K_{\theta,k+1}$ is the Kalman filter gain for parameter estimation, $\eta_{\theta,k}$ is the measured normal force, and the output matrix is

$$C_{\theta,k} = \left.\frac{\partial h_\theta^T(\xi_k, \theta)}{\partial \theta}\right|_{(\hat{\xi}_k, \hat{\theta}_k)} = \begin{bmatrix} 1 & \hat{x}_{\perp k} & \dot{\hat{x}}_{\perp k} \end{bmatrix}. \tag{9}$$

### D. Interaction Control

To enable the robot to smoothly track a predefined trajectory $r = [x_{\perp r}, x_{\parallel r}]^T$ during interaction with an environment, an interaction controller using the estimated mechanical parameters is defined through

$$u = \iota + \phi\,. \tag{10}$$

The feedforward component $\iota$ compensates for the interaction force using the predictive model (2). It is updated recursively

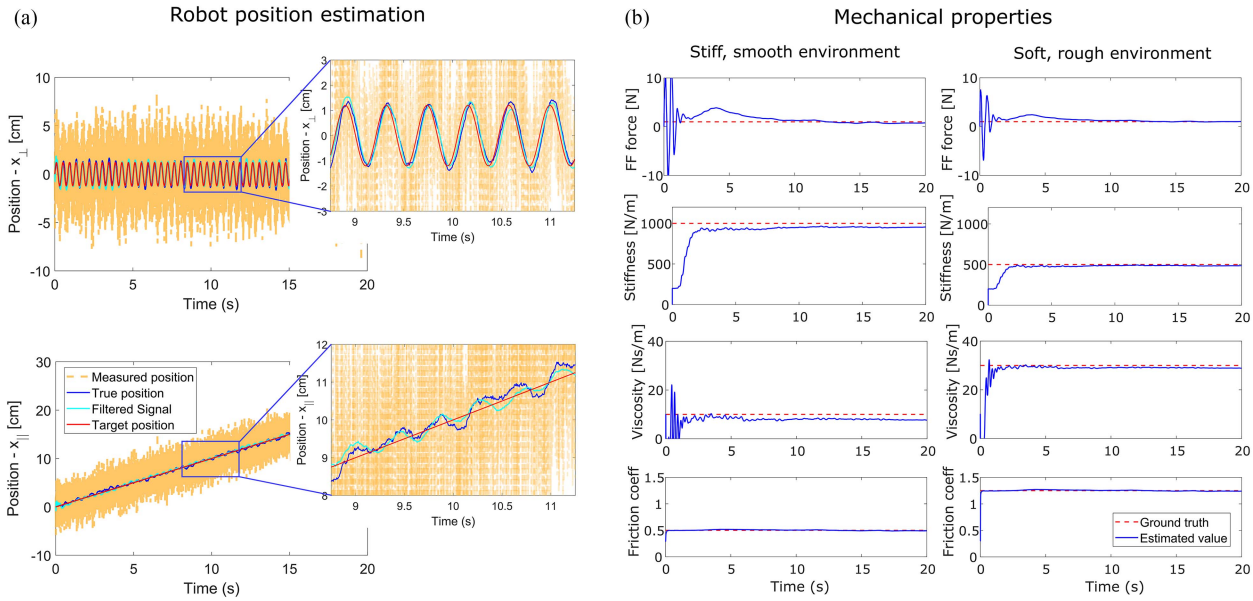


Fig. 3. Estimator in simulation. (a) Filtering of the robot position in the normal (top) and tangential (bottom) directions. (b) Estimated mechanical properties of the two environments. From top to bottom: feedforward force, stiffness, viscosity and friction coefficient.

with the estimated mechanical properties according to

$$\iota = -\begin{bmatrix} \hat{F}_\perp \\ \hat{F}_\parallel \end{bmatrix}. \tag{11}$$

The feedback component to track the target trajectory is defined as

$$\phi = -K_P\, e - K_D\, \dot{e} \tag{12}$$

with the error $e = x - r$ and control gains $K_P$ and $K_D$. To avoid overloading while in contact with a stiff surface, the control input is saturated: $\tilde{u} = sat_M(u)$ with

$$sat(s) = \begin{cases} s & |s| \le M \\ -M & s < -M < 0 \\ M & s > M > 0\,. \end{cases} \tag{13}$$

## III. Validation of Mechanical Property Estimation

### A. Simulation

We first tested the designed estimator by simulating a robot interacting with different environments. The desired trajectory was designed as

$$r = \begin{bmatrix} x_{\perp r} \\ x_{\parallel r} \end{bmatrix} = \begin{bmatrix} 0.012\sin(15t) \\ 0.01t \end{bmatrix} m\,, \quad t \in [0, 20]\, s. \tag{14}$$

A sinusoidal motion was used in the normal direction (satisfying the persistent excitation condition [37]) to ensure that the estimator had suitable information to capture the viscoelastic parameters. The amplitude and frequency were adjusted according to the allowed surface deformation. In the tangential direction, sliding with constant speed was used to yield a homogeneous lateral contact.

Two objects with different mechanical properties were considered: a stiff-and-smooth surface with $\{F_0 = 1$ N, $k = 1000$ N/m, $d = 10$ Ns/m, $\mu = 0.5\}$ and a soft-and-rough surface with $\{F_0 = 1$ N, $k = 500$ N/m, $d = 30$ Ns/m, $\mu = 1.25\}$. The control and estimation parameters used in the simulations were $\{K_P = 1000$ kg/s$^2$, $K_D = 200$ kg/s, $P_{\xi,0} = 10\, I_5$, $P_{\theta,0} = 5\, I_3$, $\triangle = 0.001$ s$\}$, where $I_5$, $I_3$ are identity matrices, sensory noise covariance R $= 4 \times 10^{-4}$, process noise covariance Q $= 2.5 \times 10^{-3} I_5$.

TABLE I
Average Value of the Mechanical Parameters in the Interval [10, 20] s Obtained by the Estimator in Simulation

| Object surface | Estimated values (ground truth values) | | |
|---|---|---|---|
| | $\hat{\kappa}$ [N/m] | $\hat{d}$ [Ns/m] | $\hat{\mu}$ |
| stiff and smooth | 953.19 (1000) | 7.97 (10) | 0.49 (0.5) |
| soft and rough | 487.20 (500) | 29.04 (30) | 1.24 (1.25) |

Fig. 3(a) shows that the estimator obtained a close estimate of the true position and velocity despite the large measurement noise. The estimated kinematic values were then passed back to the controller. As a result, the robot could track the target positions during the interaction with both environments. The estimated mechanical properties of the objects are shown in Fig. 3(b). The estimation stabilized after an approximately 2 s settling period to a value close to the ground truth (shown in Table I) for all mechanical properties in both the stiff and compliant environments. This shows that the mechanical properties can be estimated together with the robot states for different objects. Note that the coefficient of restitution was not estimated as it is not involved in the continuous interaction and computed directly from (3).

### B. Experimental Validation

The designed estimator was experimentally validated using the HMan robot [38], which is a 2-DOF cable-driven planar

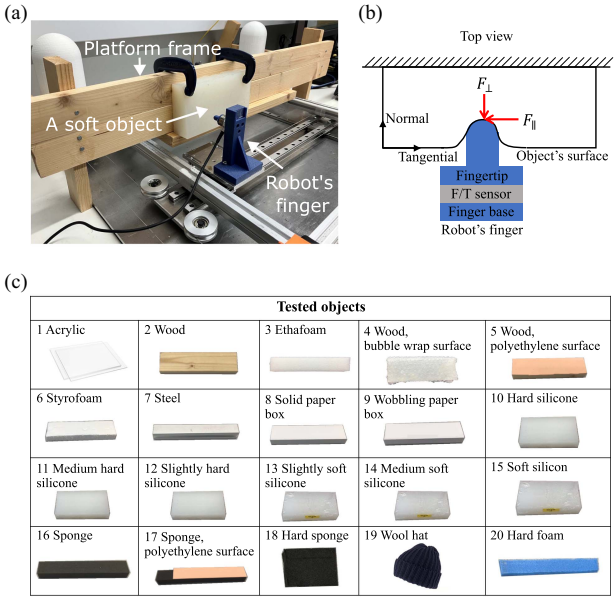


Fig. 4. Experimental setup. (a) HMan robot with a sensorized finger and an object to examine. A wooden platform frame is used to attach various objects for the robot to explore. The finger is driven by two motors in the normal and tangential directions to the object surface. (b) Diagram of the robot finger interacting with an object's surface. (c) 20 objects used in the experiment.

robot with a 24 $\times$ 28 cm$^2$ rectangular workspace controlled by two actuators (model 352699; Maxon Motor). These two actuators were controlled by a NI real-time system with a 1 kHz sampling rate. A finger was installed on the base of the robot end-effector (Fig. 4(a)), and a six-axis force sensor (SI-25-0.25; ATI Industrial Automation) was mounted between the tip and robot finger base (Fig. 4(b)) to measure the interaction forces. The finger interacted with objects attached vertically to a wooden frame. This allowed the robot to estimate the object's mechanical properties with minimal influence of gravity. Note that the tangential force was measured but not used by the estimator which only needs normal force information.

The robot interacted with 20 objects, each with a relatively flat surface to minimise the shape's influence, as shown in Fig. 4(c). These selected objects encompass a range of mechanical properties from compliant to stiff objects and smooth to rough surfaces, where the objects sometimes have similar values for a given mechanical property. This is to build a database of different objects' mechanical characteristics.

The estimator was implemented on the robot to estimate the mechanical properties of the tested objects. The experiment procedure and actions used for the estimation were as follows:

- *Tapping:* Tapping was performed initially to estimate the coefficient of restitution. To ensure that the robot had a consistent speed while approaching an object surface, a constant force was exerted to it for 0.5 seconds. Afterwards, it moved freely towards the object's surface and made an impulse.
- *Indentation:* The robot finger then started pressing the object's surface in the normal direction with a desired trajectory $x_{\perp r}(t) = 0.01\sin(8t) + 0.01\,m, t \in [0, 20]\ s$ to estimate the surface viscoelasticity. Due to hysteresis in the object's deformation, the frequency of the sinusoidal movement compared to simulations was reduced such that the robot finger would have sufficient contact with the surface. For stiff objects, the trajectory would not be followed due to control saturation (eq. (13)). to avoid large interaction force.
- *Sliding:* The robot executed a tangential sliding motion along the surface of the object at a constant velocity of 0.04 m/s, while concurrently applying a constant normal force of 4 N to estimate the coefficient of friction. To account for variations in the mechanical properties of the objects, separate movements of indentation and sliding were performed in the experiment, thereby allowing the robot to interact more smoothly with all objects.

The actions were used for all tested objects to standardize the measuring process. The estimation was validated through 25 trials for each pair of actions and object. The demonstration video can be found at[1].

### C. Estimated Mechanical Properties

To evaluate the quality of the viscoelasticity and friction coefficient estimation using only normal force data, we compared the estimation with the mechanical parameters identified from using a least squares estimator with both normal and tangential force [30], [39].

As shown in Fig. 5(a), (b), the estimated stiffness and viscosity of the compliant objects were close while using these two methods, where the root-mean-square error (RMSE) between them was 60.9 N/m for the stiffness and 0.94 Ns/m for the viscosity. The estimated viscoelasticity for hard objects is not shown because the robot could not follow the desired trajectories due to the block of the objects, leading to infeasible estimation in both methods.

To capture the friction force between the finger and objects, the robot friction was identified and subtracted from the estimator. Fig. 5(c) shows the estimated friction coefficient of all objects. The two methods exhibited similar results with an RMSE of 0.19 except {soft, medium soft, slightly soft, and slightly hard silicone}. This bias may be caused by unconsidered factors in the tangential force model, which will be further discussed.

Fig. 5(d) shows the estimated coefficient of restitution, which was directly computed from eq. (3) using force and velocity data during tapping. These estimated values suggest that although some mechanical properties are similar between objects, a combination of them may possess sufficient variability for unique object recognition.

## IV. Object Recognition

Object recognition was performed using the experimental data of Section III-B. The estimated coefficient of restitution was directly used as a feature. The mean values of the estimated stiffness, viscosity and friction coefficient from the last two

[1][Online]. Available: https://youtu.be/vE244htxuzk

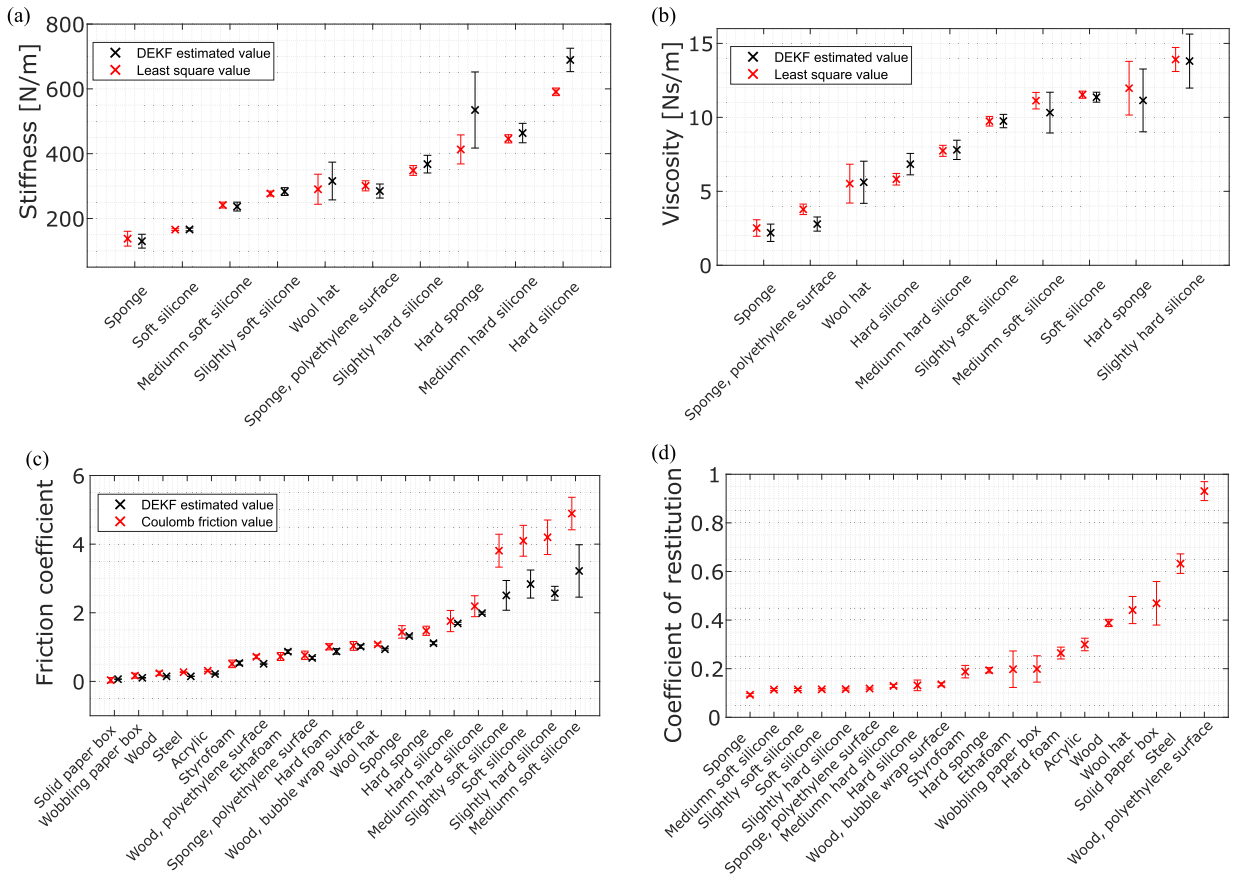


Fig. 5. The estimated mechanical property values of example tested objects (a) stiffness from soft object group (b) viscosity from soft object group (c) friction coefficient from all objects (d) coefficient of restitution from all objects.

seconds of interaction were used to extract the steady-state values as additional features.

To compare the object recognition enabled by the mechanical property features with that of previous methods used in the literature, 35 such statistical features were extracted from the raw force data. These included the mean and maximum values, and the standard deviation (sd) from the interaction force in each direction as well as from their magnitude. In addition, a value of the normal interaction force from the first contacts was used as another feature (referred to as the "tap peak"). The frequency spectrum of the force in both directions was obtained using a fast-Fourier transformation (FFT), which was averaged into four frequency bands: [0, 35], [36, 65], [66, 100] and [101, 500] Hz, where these intervals were identified during a preliminary data examination to characterise the interaction. The mean values of vibration amplitude for the frequency bands were also used as features.

To avoid overfitting, the statistical features were ranked using a feature selection method. The Chi-square test was applied since it is commonly used to evaluate features by testing their independence from the class label.

The empirical mechanical properties of the previous methods were modified and calculated to form two additional feature sets. Consistent with [7], in the first feature set the object stiffness and surface properties features in [7] were calculated based on the interaction force. In the second feature set, object compliance from [15] was calculated based on the contact force using a force/torque sensor instead of the originally considered impedance sensing electrode. The object surface properties in [15], [40] were calculated using the vibration of the dynamic interaction force instead of the dynamic pressure signal in the original work (further details are provided in section 1 of the supplementary material).

In summary, the five object recognition feature sets were formed from the mechanical property features, statistical features and empirical mechanical property features shown in Table II.

The object recognition performance of these feature sets were evaluated using both supervised and unsupervised learning methods as described in Table III. For classification, the Naive Bayes classifier was selected as it exhibited superior performance than other classifiers for supervised learning (see section 2 of the supplementary materials).

To investigate clustering, Gaussian mixture models (GMMs) were used for unsupervised learning. Clustering performance was evaluated by comparing the results with the known labels using the normalised mutual information (NMI) defined as:

$$\text{NMI} = \frac{2\,MI(C;L)}{H(C)+H(L)} \tag{15}$$

TABLE II
FEATURE SETS USED FOR OBJECT RECOGNITION

| Denomination | Features |
|---|---|
| MP: Mechanical properties | Estimated stiffness, viscosity, friction coefficient, coefficient of restitution. |
| SF: Statistical features | 35 statistical features. |
| CSSF: Chi-square test statistical features | The first 4 statistical features ranked by Chi-square test; tap peak, mean $F_{\parallel}$ obtained by sliding, std magnitude obtained by pressing, mean $F_{\perp}$ obtained by pressing. |
| EMP1 : Empirical mechanical properties feature 1 | 1 feature for stiffness, 3 features for surface texture, [7]. |
| EMP2 : Empirical mechanical properties feature 2 | 2 features for compliance and texture, [15]. 2 features for surface roughness and fineness, [40]. |

TABLE III
LEARNING METHODS, RECOGNITION ALGORITHMS, AND DATASET USED FOR CLASSIFICATION

| Method | Algorithm | Dataset[1] |
|---|---|---|
| Supervised | Naive Bayes | MP SF CSSF EMP1 EMP2 |
| Unsupervised | GMMs | |

[1]The abbreviations are defined in Table II.

where $MI(C;L)$ is the mutual information between a set of clustering results $C = \{c_1, c_2, \ldots c_N\}$ and known labels $L = \{l_1, l_2, \ldots l_N\}$:

$$MI(C;L) = \sum_i \sum_j p(c_i \cap l_j) \log \frac{p(c_i \cap l_j)}{p(c_i) \cdot p(l_j)} \tag{16}$$

and $H(\cdot)$ is the entropy

$$H(X) = -\sum_{x \in X} p(x) \log p(x)\,. \tag{17}$$

The NMI evaluates how random the generated clusters are with respect to the known labels in a range of [0, 1], where 1 means the clusters are perfectly generated according to the known labels and 0 that they are generated randomly.

### A. Classification With Mechanical Properties

To understand how each of the estimated mechanical properties impact object classification, a classification using all combinations of the mechanical features was performed. The classification was evaluated through a four-fold cross-validation using a 3:1 train:test ratio with 100 repetitions.

Fig. 6 shows the object recognition confusion matrix results using the (a) friction coefficients, (b) stiffness and viscosity, (c) coefficient of restitution, (d) friction coefficients, stiffness, and viscosity and (e) all estimated mechanical properties. It can be seen that by using only friction or the coefficient of restitution, the recognition rate is lower than 50%. These features recognise hard objects (classes 1–9 and 20) better than soft objects (classes 10–19) as shown in Fig. 6(a), (c). Using just stiffness and viscosity leads to a higher recognition rate 74.45%, but could not differentiate hard objects (Fig. 6(b)).

Fig. 6(d) shows that by combining parameters estimated with the dual Kalman filter (friction coefficient and viscoelasticity), the recognition rate can reach 89.96%, improving the results compared to using a single mechanical feature. However, there is still some confusion within the stiff objects due to similar friction, e.g. wood (class 2) and steel (class 7).

After integrating the estimated coefficient of restitution, using all four mechanical properties in the classifier further increased the recognition rate to 98.18% (Fig. 6(e)). The resulting confusion matrix exhibits almost perfect recognition with a rate over 90% for each object. Although there is some confusion between pairs of object class, the misclassification rate of each object is lower than 0.05%, which can be considered as negligible. These results demonstrate the advantages provided by using the combination of different mechanical properties, especially including the coefficient of restitution, to classify various objects. The recognition rates for all combinations of mechanical features are provided in section 3 of the supplementary material.

### B. Object Classification With Mechanical Properties Vs. Statistical Features

To examine the role of using the estimated mechanical properties for object classification compared to other feature sets, the classifier was used to find the recognition rates from the five sets of features described in Table III: mechanical property features (MP), statistical features (SF and CSSF) and empirical mechanical properties features (EMP1 and EMP2). These object classifications were evaluated by a four-fold cross-validation using 100 repetitions.

Fig. 7(a) shows that using mechanical properties as features resulted in a recognition rate of $98.18 \pm 0.424\%$. On the other hand, the statistical features with and without feature selection resulted in a recognition rate of $92.2 \pm 0.60\%$ and $89.7 \pm 3.20\%$ respectively. Lastly, the EMP1 features used in [7] provided $77.5 \pm 5.07\%$ and the EMP2 features used in [40] and [15] yielded $82.9 \pm 0.91\%$. These results show that mechanical properties provided the highest recognition rate while using a lower number of features and without needing tangential force sensing.

### C. Object Clustering Using Mechanical Properties or Statistical Features

To study the benefit of using the coefficient of restitution, stiffness, viscosity and friction coefficient together in an unsupervised learning method, GMMs clustering was used with the same five sets of feature as in Section IV-B. We assumed that each cluster had its own diagonal covariance matrix and that the number of clusters was set to 20, i.e. the number of tested objects. This clustering task was carried out and evaluated by NMI for 40 repetitions for each set of features.

The evaluation of clustering results using NMI is shown in Fig. 7(b). Using mechanical features gave NMI values of $0.851 \pm 0.03$ which is similar to what the SF and CSSF provided at $0.863 \pm 0.016$ and $0.856 \pm 0.018$ respectively ($p > 0.05$,

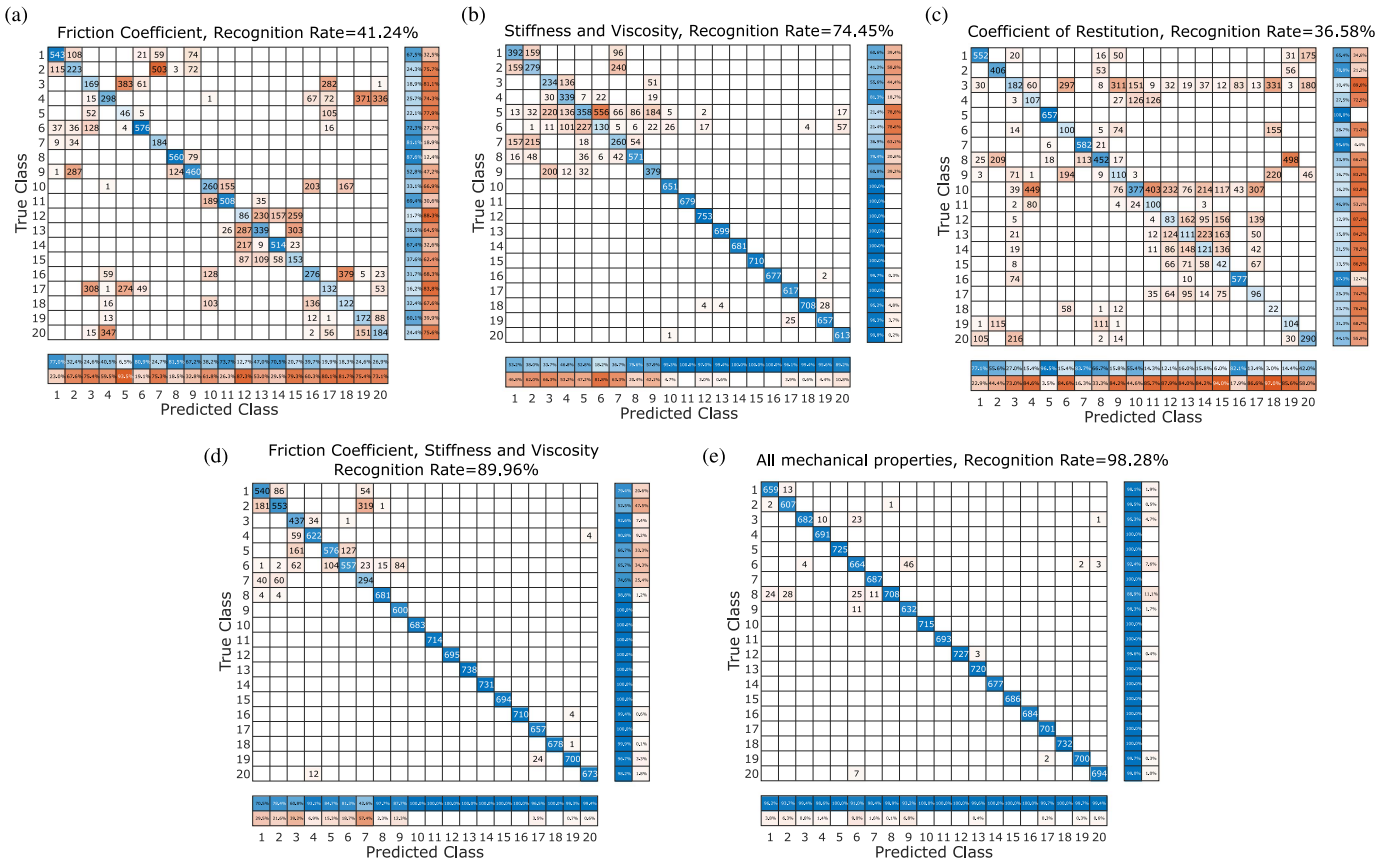


Fig. 6. Confusion matrix obtained by using (a) friction coefficient (b) stiffness and viscosity (c) coefficient of restitution (d) friction coefficient, stiffness and viscosity (e) all mechanical properties as features. Blue corresponds to correct classified objects while red corresponds to incorrect classified objects.

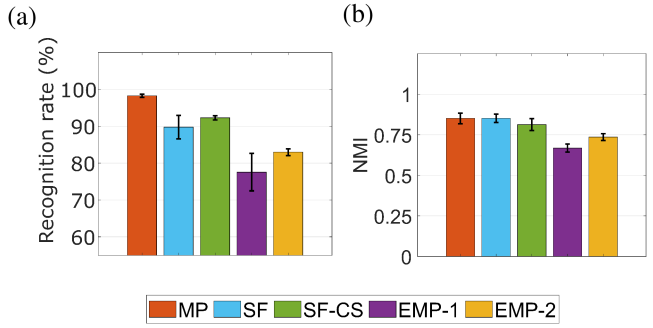


Fig. 7. Classification (a) and clustering using the NMI (b) for the different feature sets described in Table III.

Dunn's test). However, the NMI results obtained using the MP were found to be higher than the results obtained using EMP1 and EMP2. This suggests that using four mechanical properties could provide the same results as with 35 statistical features, and outperform the other features representing empirical mechanical properties used in [7], [15], [40].

## V. Discussion

This paper introduced an object recognition framework based on the estimation of mechanical properties with a dual extended Kalman filter. This online method extends [34] and stably estimates the coefficient of restitution, stiffness, viscosity and friction parameters. The method's viability was demonstrated in simulations and experiments. Our estimator using only the normal force yielded mechanical property parameters that were comparable to those estimated using both the normal and tangential forces, showing that mechanical features that can be leveraged for object recognition.

The classification performance was evaluated with the obtained experimental data. Using the four representative mechanical parameters, a recognition rate of 98.18 $\pm$ 0.424% could be achieved using supervised learning, and clustering exhibited a normalized mutual information of 0.851 $\pm$ 0.03. Using only four mechanical parameters resulted in a better classification and similar clustering as with 35 statistical features, suggesting that mechanical features entail a more compact and accurate representation than statistical features.

The coefficient of restitution, viscoelastic and friction parameters were all required to distinguish objects. In particular, including the coefficient of restitution largely improved the recognition rate compared to using only viscoelastic parameters. For example, using stiffness could not distinguish steel from wood as both are hard materials, but they had different impact properties as measured by the coefficient of restitution.

The intrinsic mechanical properties estimated in our scheme provided better and more consistent results than the empirical mechanical properties used in previous works [7], [15], [40]. This illustrates the limitations of using empirical features to recognize objects, which may depend on the specific action used. For instance, the surface texture measure of [15], defined as a variance of the interaction force in the normal direction while the robot finger slid on object surface, leads to inconsistent estimation results because its value may depend on the object pose and robot interaction.

Despite the promising results of this study, some limitations should be acknowledged. First, although the current Coulomb model extracts the surface friction property well for stiff objects, the estimation was less accurate for compliant objects as the lateral interaction is more affected by the material deformation. This could be addressed using a more sophisticated tangential interaction force model to represent a versatile representation of the lateral interaction force. Second, in our experiments, we primarily used objects with flat surfaces to minimize the influence of shape on the results. For objects with curved surfaces, the method needs to be extended to estimate their mechanical properties by integrating a contour following algorithm e.g. [41].

In summary, this work emphasized the role of mechanical properties in haptic exploration, and how they can be used to reliably recognise different objects. The results demonstrated the superiority of the mechanical properties-based object recognition, yielding more reliable recognition than empirical properties and requiring far less features than based on statistical features. It is noteworthy that the coefficient of restitution during impact can distinguish otherwise similar materials, e.g. solid materials such as wood and steel. Moreover, using this intrinsic object representation makes the framework flexible to using various classification algorithms. While the presented system could successfully recognize objects during haptic exploration, considering the weight and inertial parameters would enable extending our framework from haptic exploration to enabling full object manipulation with transport.

## REFERENCES


[1] S. Luo, J. Bimbo, R. Dahiya, and H. Liu, "Robotic tactile perception of object properties: A review," *Mechatronics*, vol. 48, pp. 54–67, 2017. [Online]. Available: http://www.sciencedirect.com/science/article/pii/S0957415817301575

[2] P. K. Allen and K. S. Roberts, "Haptic object recognition using a multi-fingered dextrous hand," in *Proc. IEEE Int. Conf. Robot. Autom.*, 1989, pp. 342–347.

[3] U. Martinez-Hernandez, T. J. Dodd, and T. J. Prescott, "Feeling the shape: Active exploration behaviors for object recognition with a robotic hand," *IEEE Trans. Syst. Man Cybern. Syst*, vol. 48, no. 12, pp. 2339–2348, Dec. 2018.

[4] Z. Pezzementi, E. Plaku, C. Reyda, and G. D. Hager, "Tactile-object recognition from appearance information," *IEEE Trans. Robot.*, vol. 27, no. 3, pp. 473–487, Jun. 2011.

[5] J. Hoelscher, J. Peters, and T. Hermans, "Evaluation of tactile feature extraction for interactive object recognition," in *Proc. IEEE-RAS 15th Int. Conf. Humanoid Robots*, 2015, pp. 310–317.

[6] P. Dallaire, P. Giguère, D. Émond, and B. Chaib-Draa, "Autonomous tactile perception: A combined improved sensing and Bayesian non-parametric approach," *Robot. Auton. Syst.*, vol. 62, no. 4, pp. 422–435, 2014. [Online]. Available: http://www.sciencedirect.com/science/article/pii/S0921889013002285

[7] M. Kaboli, K. Yao, D. Feng, and G. Cheng, "Tactile-based active object discrimination and target object search in an unknown workspace," *Auton. Robots*, vol. 43, no. 1, pp. 123–152, 2019, doi: 10.1007/s10514-018-9707-8.

[8] W. J. Stronge, *Impact Mechanics*, 2nd ed. Cambridge, U.K.: Cambridge Univ. Press, 2018.

[9] A. Rebguns, D. Ford, and I. Fasel, "Infomax control for acoustic exploration of objects by a mobile robot," in *Proc. AAAI Conf. Lifelong Learn.*, 2011, pp. 22–28.

[10] M. Neumann, K. Nottensteiner, I. Kossyk, and Z. C. Marton, "Material classification through knocking and grasping by learning of structure-borne sound under changing acoustic conditions," in *Proc. IEEE 14th Int. Conf. Automat. Sci. Eng.*, 2018, pp. 1269–1275.

[11] S. Luo, L. Zhu, K. Althoefer, and H. Liu, "Knock-knock: Acoustic object recognition by using stacked denoising autoencoders," *Neurocomputing*, vol. 267, pp. 18–24, Dec. 2017, doi: 10.1016/j.neucom.2017.03.014.

[12] N. Roy, G. Dudek, and P. Freedman, "Surface sensing and classification for efficient mobile robot navigation," in *Proc. IEEE Int. Conf. Robot. Autom.*, 1996,pp. 1224–1228.

[13] P. Wisanuvej, J. Liu, C. M. Chen, and G. Z. Yang, "Blind collision detection and obstacle characterisation using a compliant robotic arm," in *Proc. IEEE Int. Conf. Robot. Autom.*, 2014, pp. 2249–2254.

[14] J. Windau and W. M. Shen, "An inertia-based surface identification system," in *Proc. IEEE Int. Conf. Robot. Autom.*, 2010, pp. 2330–2335.

[15] D. Xu, G. E. Loeb, and J. A. Fishel, "Tactile identification of objects using Bayesian exploration," in *Proc. IEEE Int. Conf. Robot. Autom.*, 2013, pp. 3056–3061.

[16] A. J. Spiers, M. V. Liarokapis, B. Calli, and A. M. Dollar, "Single-grasp object classification and feature extraction with simple robot hands and tactile sensors," *IEEE Trans. Haptics*, vol. 9, no. 2, pp. 207–220, Apr.–Jun. 2016.

[17] Z. Su, J. Fishel, T. Yamamoto, and G. Loeb, "Use of tactile feedback to control exploratory movements to characterize object compliance," *Front. Neurorobot.*, vol. 6, 2012, Art. no. 7. [Online]. Available: https://www.frontiersin.org/article/10.3389/fnbot.2012.00007

[18] M. Bednarek, P. Kicki, J. Bednarek, and K. Walas, "Gaining a sense of touch object stiffness estimation using a soft gripper and neural networks," *Electron.*, vol. 10, no. 1, 2021, Art. no. 96. [Online]. Available: https://www.mdpi.com/2079-9292/10/1/96

[19] S. Chitta, J. Sturm, M. Piccoli, and W. Burgard, "Tactile sensing for mobile manipulation," *IEEE Trans. Robot.*, vol. 27, no. 3, pp. 558–568, Jun. 2011.

[20] L. J. Love and W. J. Book, "Environment estimation for enhanced impedance control," in *Proc. IEEE Int. Conf. Robot. Autom.*, 1995, vol. 2, pp. 1854–1859.

[21] A. Ren, C. Qi, F. Gao, X. Zhao, and Q. Sun, "Contact stiffness identification with delay and structural compensation for hardware-in-the-loop contact simulator," *J. Intell. Robot. Syst.*, vol. 86, pp. 1–9, 2017.

[22] R. Rossi, L. Fossali, A. Novazzi, L. Bascetta, and P. Rocco, "Implicit force control for an industrial robot based on stiffness estimation and compensation during motion," in *Proc. IEEE Int. Conf. Robot. Autom.*, 2016, pp. 1138–1145.

[23] P. Chalasani, L. Wang, R. Yasin, N. Simaan, and R. H. Taylor, "Preliminary evaluation of an online estimation method for organ geometry and tissue stiffness," *IEEE Robot. Automat. Lett.*, vol. 3, no. 3, pp. 1816–1823, Jul. 2018.

[24] K. Yane and T. Nozaki, "Recognition of environmental impedance configuration by neural network using time-series contact state response," in *Proc. IEEE Int. Conf. Adv. Motion Control*, 2022, pp. 426–431.

[25] S. Huang and H. Wu, "Texture recognition based on perception data from a bionic tactile sensor," *Sensors*, vol. 21, no. 15, 2021, Art. no. 5224. [Online]. Available: https://www.mdpi.com/1424-8220/21/15/5224

[26] V. Chu et al., "Robotic learning of haptic adjectives through physical interaction," *Robot. Auton. Syst.*, vol. 63, pp. 279–292, 2015. [Online]. Available: https://www.sciencedirect.com/science/article/pii/S0921889014002061

[27] J. Sinapov, V. Sukhoy, R. Sahai, and A. Stoytchev, "Vibrotactile recognition and categorization of surfaces by a humanoid robot," *IEEE Trans. Robot.*, vol. 27, no. 3, pp. 488–497, Jun. 2011.

[28] B. Sundaralingam and T. Hermans, "In-hand object-dynamics inference using tactile fingertips," *IEEE Trans. Robot.*, vol. 37, no. 4, pp. 1115–1126, Aug. 2021.

[29] Z. Su et al., "Force estimation and slip detection/classification for grip control using a biomimetic tactile sensor," in *Proc. IEEE-RAS 15th Int. Conf. Humanoid Robots*, 2015, pp. 297–303.

[30] T. Sun, J. Back, and H. Liu, "Combining contact forces and geometry to recognize objects during surface haptic exploration," *IEEE Robot. Automat. Lett.*, vol. 3, no. 3, pp. 2509–2514, Jul. 2018.
[31] C. Canudas de Wit, H. Olsson, K. Astrom, and P. Lischinsky, "A new model for control of systems with friction," *IEEE Trans. Autom. Control*, vol. 40, no. 3, pp. 419–425, Mar. 1995.
[32] X. Song, H. Liu, J. Bimbo, K. Althoefer, and L. D. Seneviratne, "Object surface classificaiton based on friction properties for intelligent robotic hands," in *Proc. World Automat. Congr.*, 2012, pp. 1–5.
[33] H. Liu, X. Song, J. Bimbo, L. Seneviratne, and K. Althoefer, "Surface material recognition through haptic exploration using an intelligent contact sensing finger," in *Proc. IEEE/RSJ Int. Conf. Intell. Robots Syst.*, 2012, pp. 52–57.
[34] Y. Li, G. Ganesh, N. Jarrassé, S. Haddadin, A. Albu-Schaeffer, and E. Burdet, "Force, impedance, and trajectory learning for contact tooling and haptic identification," *IEEE Trans. Robot.*, vol. 34, no. 5, pp. 1170–1182, Oct. 2018.
[35] F. G. Pfeiffer and C. Glocker, "On frictionless impact models in rigid-body systems," *Philos. Trans. Roy. Soc. London. Ser. A: Math., Phys. Eng. Sci.*, vol. 359, no. 1789, pp. 2385–2404, 2001, doi: 10.1098/rsta.2001.0857.
[36] E. A. Wan and A. T. Nelson, "Dual extended Kalman filter methods," in *Kalman Filtering and Neural Networks*. Hoboken, NJ, USA: Wiley, 2001, pp. 123–173.
[37] P. A. Ioannou and J. Sun, *Robust Adaptive Control*, vol. 1, Upper Saddle River, NJ: PTR Prentice-Hall, 1996.
[38] D. Campolo, P. Tommasino, K. Gamage, J. Klein, C. M. Hughes, and L. Masia, "H-man: A planar, h-shape cabled differential robotic manipulandum for experiments on human motor control," *J. Neurosci. Methods*, vol. 235, pp. 285–297, 2014. [Online]. Available: https://www.sciencedirect.com/science/article/pii/S0165027014002477
[39] D. Erickson, M. Weber, and I. Sharf, "Contact stiffness and damping estimation for robotic systems," *Int. J. Robot. Res.*, vol. 22, no. 1, pp. 41–57, 2003.
[40] J. Fishel and G. Loeb, "Bayesian exploration for intelligent identification of textures," *Front. Neurorobot.*, vol. 6, 2012, Art. no. 4. [Online]. Available: https://www.frontiersin.org/article/10.3389/fnbot.2012.00004
[41] J. Back, J. Bimbo, Y. Noh, L. Seneviratne, K. Althoefer, and H. Liu, "Control a contact sensing finger for surface haptic exploration," in *Proc. IEEE Int. Conf. Robot. Autom.*, 2014, pp. 2736–2741.